

# We are IntechOpen, the world's leading publisher of Open Access books Built by scientists, for scientists

6,900

Open access books available

185,000

International authors and editors

200M

Downloads

Our authors are among the

154

Countries delivered to

TOP 1%

most cited scientists

12.2%

Contributors from top 500 universities



WEB OF SCIENCE™

Selection of our books indexed in the Book Citation Index  
in Web of Science™ Core Collection (BKCI)

Interested in publishing with us?  
Contact [book.department@intechopen.com](mailto:book.department@intechopen.com)

Numbers displayed above are based on latest data collected.  
For more information visit [www.intechopen.com](http://www.intechopen.com)



# Synthesis of Nanostructured Hydroxyapatite via Controlled Hydrothermal Route

*Andrea Ruffini, Simone Sprio, Lorenzo Preti  
and Anna Tampieri*

## Abstract

Hydroxyapatite represents the natural inorganic component of the bone and may be considered an essential element required for the development of bone substitutes in the field of regenerative medicine. Hydroxyapatite bone substitutes own biomimetic, osteoconductive, and osteoinductive properties thanks to their chemical-physical properties and nanostructure that play a critical role for the reconstruction of calcified tissues. Controlling the structure of hydroxyapatite nanocrystals is vital for obtaining a sustained product, and it should be an advantage on the final materials suitable for bone replacement, in terms of adsorptive activity, drug delivery system, etc. Compared to other synthesis techniques, hydrothermal processing (refers to a synthesis in aqueous solution at elevated pressure and temperature, in a closed system) has the ability to precipitate the hydroxyapatite from overheated solution, regulating the rate and uniformity of nucleation, growth, and maturation, which affect size, morphology, and aggregation of the crystals. This chapter wants to provide an overview of realization of nanosized hydroxyapatite-based bioceramics (e.g., powder and 3D structures) with desired morphology of crystallites, by hydrothermal processing. In this way, some critical hydrothermal parameters fundamental on the control of the crystal shape and dimension (pH, temperature, starting precursors, etc.) are discussed.

**Keywords:** hydrothermal synthesis, nanostructured hydroxyapatite, crystal growth, morphology control, regenerative medicine

## 1. Introduction

Calcium phosphates (CaP) are the main mineral constituent of human bones and teeth. For this reason, synthetically CaP-based materials nowadays are the most ubiquitous family of biomaterials for their use in biological applications and tissue engineering. These attractive biomedical materials possess excellent biocompatibility, osteoconductive properties, nontoxicity, and chemical similarity to the inorganic component of the natural bone [1].

The realization of CaP biomaterials reproducing the calcified tissue (dense and porous block, granules, and powders) is clinically needed as an alternative to

autologous- and heterologous-derived scaffolds [2]. The majority of CaP biomaterials shall be applicable for bone reconstruction and replacement in tissue engineering when the bone has no self-regenerative capacity following severe illness or trauma, as well as other applications, like drug delivery agents, prosthetic coatings, and gene carriers [3, 4].

Among the CaP family compounds, hydroxyapatite  $\text{Ca}_5(\text{PO}_4)_3\text{OH}$  (HA) is the most extensively used in medicine for implant fabrication as an alternative to the human bone; it is the thermodynamically most stable phase in physiological conditions and owns the most similarity in mineralogical phase and chemical composition to the mineral part of the bone tissue [5]. The *in vivo* formation of this mineral occurs through the biomineralization process, where nanometer-sized crystals of HA are precipitated on collagen fibrils into mineralized self-assembled hierarchical and calcified structure. The thickness of the HA crystals ranges from about 5 to 20 nm, while the length from 15 to 200 nm [6].

Biological HA is a nonstoichiometric, carbonated, and calcium-deficient form of apatite (Ca/P atomic ratio lower than 1.67), containing various amounts of positively charged ions (e.g.,  $\text{Mg}^{2+}$ ,  $\text{Na}^+$  and  $\text{K}^+$ ) and negatively charged ions (e.g.,  $\text{CO}_3^{2-}$ ,  $\text{Cl}^-$  and  $\text{F}^-$ ), in substitution of  $\text{Ca}^{2+}$  or  $\text{PO}_4^{3-}/\text{OH}^-$  ions, respectively [7, 8].

Present-day researches concern new route or improving preexisting methods to accurately engineer HA-based materials with characteristics closer to the living bone, aiming more effective applications in the field of biomaterials. The *in vivo* and *in vitro* performance of HA biomaterials remarkably depends on the development of their properties during the manufacturing process, such as microscopic characteristic (e.g., grain size topography, particles size distribution, nanostructure), morphology (e.g., porosity, pore size, 3-D architecture), chemical compositions, crystallographic structure, etc.

It is well known that biological and mechanical properties of biomaterials are strongly affected by its nanostructural characteristics. Compared to conventional ceramic formulations, the nanophase of HA materials can significantly affect their mechanical strength and the solubility that has a substantial effect on resorption and bioactivity. Furthermore, nanostructures can enhance osteoblast adhesion and affect the surface wettability for the selective control of protein interactions [9]. The mechanical properties and microstructures of the resulting HA ceramics are mostly influenced by the microstructure of the produced powder, including crystallinity, agglomeration, stoichiometry, and substitutions and the processing conditions [10].

The control over HA crystallization through a precise control of crystal nucleation and growth is a major challenge in the synthesis of crystalline particles, with defined geometry, morphologies, orientations, sizes, and composition. These intrinsic features are closely related to their properties and may affect their applications.

Many methods have been proposed in the literature to prepare nanostructured HA materials (e.g., nanoparticles or 3-D scaffolds with various shapes and sizes), such as coprecipitation, sol-gel synthesis, mechanical milling, hydrothermal reaction, etc. [11]. Between them, hydrothermal synthesis method allows more choice of variable factors that affect the morphology of the final material, such as nature of precursors and their concentration, saturation, temperature, pH, process time, and the presence of potential agents used for controlling the final morphological structures [12, 13].

This chapter focuses on the synthetic hydrothermal strategy employed in the preparation and design of different HA nanoparticles and nanostructured materials and reviews about the roles of important parameters on the HA nanostructured realization.

2. Nanostructured hydroxyapatite

CaP exhibit different characteristics as Ca/P atomic ratios, crystal systems, and solubility (in physiological conditions,  $T = 37^{\circ}\text{C}$ ,  $\text{pH} = 7.3$ ) [14, 15]; some most common CaP used for biomedical applications are summarized in **Table 1**. CaP materials which have Ca/P atomic ratio external to 1–2 range are not suitable for implantation into the body because of their high acidity (low Ca/P), basicity (high Ca/P), and solubility. As a result, among the known CaP compounds, OCP,  $\alpha/\beta$ -TCP and CDHA/HA are significantly most useful for biomedical applications, like orthopedic surgery and dentistry.

The different crystal morphologies of CaP exhibited in the various biological hard tissue have addressed the research to develop these materials with high control of nanostructural properties, as particle size, nano-surface, dimensional anisotropy, etc. For example, in the bone tissue, the HA crystallites have rod shape owning dimension of about  $50 \times 25 \times 4 \text{ nm}$ ; in contrast, in the tooth enamel, larger hexagonal prism crystallites have the dimension of about  $100 \times 70 \times 25 \text{ nm}$ , with c-planes that are preferentially parallel to the collagen fibrils or enamel surface, respectively [16]. For this reason, crystals exhibit enhanced adsorption properties because of their higher charging surface and with plate-like and hexagonal morphologies, may find promising application in dental implants.

Lee et al. reported enhanced bioactivity of nanostructured HA compared to sintered and coarser ceramics: nanophase HA promotes the osteogenic differentiation of periodontal ligament cells and more efficiency of osteoclast-like cell adhesion [7]. Besides, HA nanoparticles are used for cell targeting, gene transfecting, and drug delivery thanks to their strong molecular adsorption property and increased surface area [17]. The size of HA particles also play critical roles in biological response, including cell proliferation modification, oriented cell differentiation, and cell apoptosis [18]. HA nanowires and nanosheets are capable for moderated reinforcement of the biomaterials and can be used as mechanical components to stiffen isotropic composite materials. In the case of sinterability of bioceramics, nanoparticles exhibit improved feature if compared to coarser particles [19].

Stoichiometric HA has typically hexagonal crystal system with the  $P6_3/m$  space group and two principal crystal planes: a-plane and c-plane (see **Figure 1**); its crystal unit cell is characterized by  $a = b = 0.942 \text{ nm}$  and  $c = 0.688 \text{ nm}$ ,  $\alpha = \beta = 90^{\circ}$  and  $\gamma = 120^{\circ}$ . Positively charged calcium ions ( $\text{Ca}^{2+}$ ) are mainly present in the a-planes,

Calcium phosphates	Acronym	Ca/P ratio	Crystal system	$K_{ps} \text{ (log)}$
Monetite, $\text{CaHPO}_4$	DCPA	1	Triclinic	7.02
Brushite, $\text{CaHPO}_4 \cdot 2\text{H}_2\text{O}$	DCPD	1	Monoclinic	6.63
Amorphous calcium phosphate, $\text{Ca}_x\text{H}_y(\text{PO}_4)_z \cdot n\text{H}_2\text{O}$ ; $3 < n < 4.5$	ACP	1.2–2.2	—	<4
Octacalcium phosphate, $\text{Ca}_8(\text{HPO}_4)_2(\text{PO}_4)_4 \cdot 5\text{H}_2\text{O}$	OCP	1.33	Triclinic	95.9
$\alpha$ -Tricalcium phosphate, $\alpha\text{-Ca}_3(\text{PO}_4)_2$	$\alpha$ -TCP	1.5	Monoclinic	25.5
$\beta$ -Tricalcium phosphate, $\beta\text{-Ca}_3(\text{PO}_4)_2$	$\beta$ -TCP	1.5	Rhombohedral	29.5
Calcium-deficient hydroxyapatite, $\text{Ca}_{5-x}(\text{HPO}_4)_x(\text{PO}_4)_{3-x}(\text{OH})$ ; $0 < x < 0.5$	CDHA	1.5–1.67	Hexagonal	<42.6
Hydroxyapatite, $\text{Ca}_5(\text{PO}_4)_3(\text{OH})$	HA	1.67	Hexagonal	58.6
Tetracalcium phosphate, $\text{Ca}_4(\text{PO}_4)_2\text{O}$	TTCP	2	Monoclinic	37–42

**Table 1.**  
Main CaP compounds used for biomedical applications.

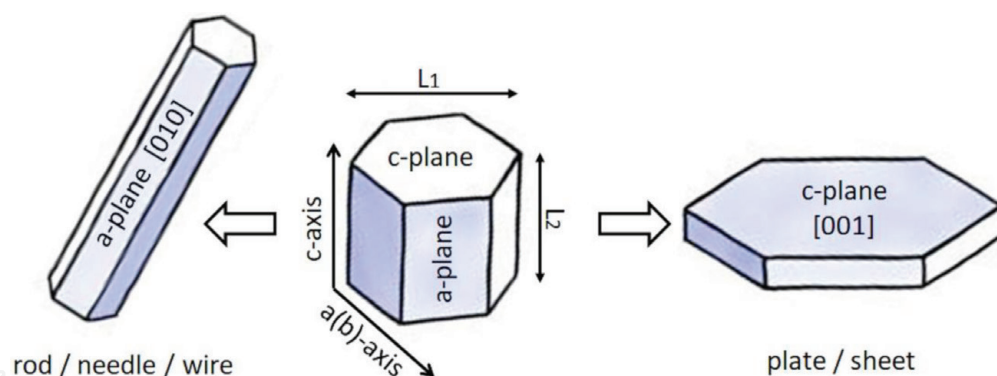


**Figure 1.** Hexagonal crystal structure of stoichiometric HA, where a-plane is Ca site (positive charge) and c-plane is  $\text{PO}_4$  site (negative charge).

and hence negatively charged phosphate ( $\text{PO}_4^{3-}$ ) and hydroxide ( $\text{OH}^-$ ) ions are present in the c-planes. That is, HA surfaces present anisotropic characteristics such as adsorption profiles for electrolytes or biomolecules [16].

### 3. Hydrothermal synthesis of calcium phosphates

The preparation of HA crystals with controlled morphology and phase pure (both in powder or scaffold forms) has been the object of intensive research over the last decades. Sadat-Shojai and Earl et al. [13, 20] summarized three main processing routes (which include specific techniques) developed for synthesizing nanosized HA:

- Dry methods (i.e., mechanochemical, solid-state reaction processes)
- Wet methods (i.e., precipitation, hydrolysis, sol-gel, hydrothermal, solvothermal, emulsion, sonochemical, microwave, chemical vapor deposition processes)
- High-temperature processes (i.e., combustion preparation, synthesis from biogenic sources)

Wet chemistry techniques are widely used for their particularly effective control of particle size, morphology, and crystallinity. Among this, the hydrothermal technique is a promising and convenient way to easily control the reaction conditions, through a one-step synthesis of a desired phase under gentle reaction conditions [21].

Byrappa and Yoshimura defined hydrothermal processing as any heterogeneous chemical reaction developed in a closed system, in the presence of an aqueous solvent and above to its boiling temperature and pressure ( $T > 100^\circ\text{C}$ ;  $P > 1 \text{ atm}$ ) and able to dissolve and recrystallize materials that are relatively insoluble under normal conditions. Other authors established hydrothermal conditions as a chemical precipitation in which the dissolution, crystal growth, and aging steps are conducted at a high temperature and pressure (typically above the water boiling point) inside an apparatus consisting of a steel pressure vessel called reactor/autoclave [21, 22]. Classically, a temperature gradient is maintained between the opposite ends of the vessel by using an external heater jacket with controlled temperature, and the pressure is measured by a gas pressure transmitter [23].

The hydrothermal technique can be effective in processes aimed to the production of highly homogeneous and monodispersed nanoparticles but also used as



attractive techniques for processing of nanostructured 3D materials. Specifically, recent studies in hydrothermal conditions were carried out on the realization of HA ceramic generated, partially or entirely, starting from various biogenic sources, such as marine algae, shell, corals, or wood [24–27]. The biomorphic transformations in hydrothermal conditions enable to create a material with the preservation of natural-starting 3D structure (similar to that human bone) and appropriate nanostructural characteristics, use as a bone graft substitute for bone implants [28].

The achieving of a precise controlling of morphology, geometry and size, over the crystallographic and chemical structure of HA in hydrothermal conditions is related with a largest range of useful work conditions, in particular the temperature. The literature reports many variety of hydrothermal methods for the realization of HA-nanostructured materials, in a wide range of dimension and variety of morphological features of the crystals, for example, rods [20, 29–46], needles [29, 30, 32, 47–53], wires [18, 54–57], whiskers/fibers [23, 47, 49, 58–60], sheets [55, 61, 62], plates [23, 44, 47–49, 54, 63, 64], and organized rod spheres [18, 31, 44, 54, 65, 66] or sheet spheres [19, 61, 67, 68], etc. (see **Table 2** and **Figure 2**). Aldrich and Smith defined a geometric nomenclature for nanoparticles [69], frequently described in ambiguous way in many scientific works; for example, the geometry indicating elongated HA as rod, needle, and fibers should be named according to well-defined dimensional aspect ratio and c-axial length.

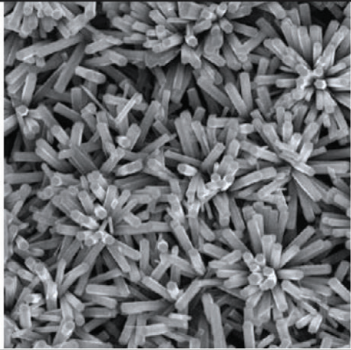
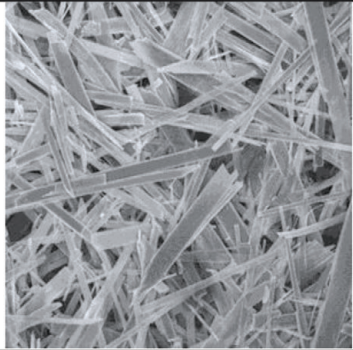
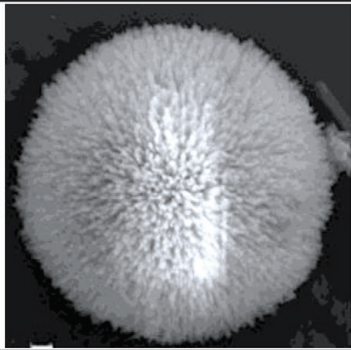
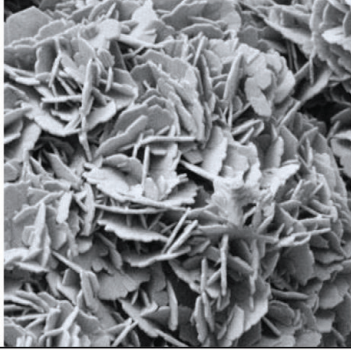
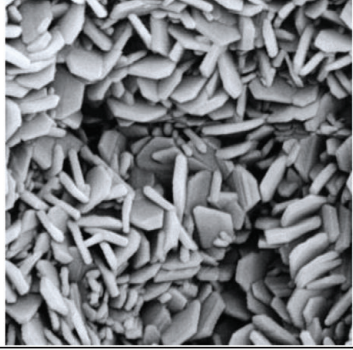
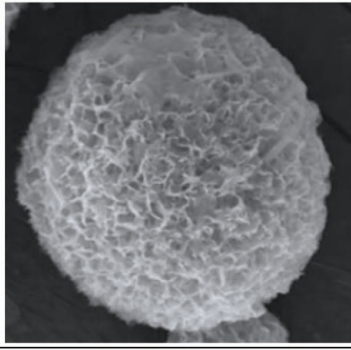
This study is mainly focused on the correlation between the different HA morphologies and stoichiometries obtained and the various parameters that affect crystallization in the hydrothermal process, with their complex relationship. Appropriate operating conditions can be carried out and adjustment to induce in the crystallization pathway and produce the desired morphology [70, 71]. Size and morphology of nanoparticles can be tailored by varying the most important synthesis conditions (described in Sections 3.1–3.7), including thermodynamic and non-thermodynamic processing variables (nature and stoichiometry of reactants, temperature, pH, pressure, process time, and additives).

3.1 Supersaturation, nucleation, and crystal growth

Supersaturation is the most critical crystallization parameter, and, at a given temperature, it is commonly related to a higher amount of a substance in solution than that required for saturation.

Long shape (L1 < L2)	Size range	L2/L1 ratio
Rod	L1 = 3 nm–300 μm	L2/L1 (rods) = 5–15
Needle	L2 = 10 nm–800 μm	L2/L1 (needles) = 20–80
Wire		L2/L1 (wires) = 50–100
Whisker/fiber	L1 = 100–1000 nm L2 = 30–100 μm	L2/L1 = 100–300
Large shape (L1 > L2)	Size range	L1/L2 ratio
Sheet	L1 = 40 nm–50 μm	L1/L2 = 10–20
Plate	L2 = 5 nm–3 μm	
Spherical shape	Size range	—
Organized rod sphere	Ø = 500 nm–100 μm	—
Organized sheet sphere		

**Table 2.**  
*Various HA nanoparticle shapes and achievable size range by hydrothermal processes (where L1 is the width and L2 is the high, (see **Figure 1**)).*

long shape (L1 < L2)		spherical shape
		
rod / needle / wire	whisker / fiber	organized rod sphere
large shape (L1 > L2)		spherical shape
		
sheet	plate	organized sheet sphere

**Figure 2.**  
*Typical shapes of nanostructured HA.*

It is the thermodynamic driving force that governs the formation mechanism of HA crystals, through nucleation and growth processes, and dictates the final crystal size distribution [44]. Nucleation and crystal growth are often competing mechanisms determining for the final crystal size and size distribution.

The thermodynamic driving force that induces the precipitation of HA under hydrothermal conditions is defined by the free energy variation in supersaturated solutions, which is given by the following relation in Eq. (1):

$$\Delta G = -(RT/n) \ln(A/K_{sp}) = -(RT/n) \ln(S) \tag{1}$$

where  $\Delta G$  is the molar Gibbs energy;  $R$  is the universal gas constant;  $T$  is the absolute temperature;  $n$  is the number of ions in HA molecule (for  $\text{Ca}_5(\text{PO}_4)_3(\text{OH})$  is  $n=5+3+1=9$ ); and  $S$  is the supersaturation degree that is defined by the activity product of ion units ( $A$ ) to the corresponding solubility product ( $K_{sp}$ ) ratio, at a given temperature. Equation (1) also leads to the conclusion that the trend of absolute  $\Delta G$  is directly related to the temperature. For example, if the temperature decreases, a slower precipitation rate of HA occurs and could lead to a larger crystal size.

The supersaturation degree ( $S$ ) is defined as Eq. (2) where  $a_A$ ,  $a_B$ , etc. are the activity of ionic species and  $K_{sp}$  is the solubility product constant. In the case of HA ( $\text{Ca}_5(\text{PO}_4)_3(\text{OH})$  or half unit cell), the supersaturation ( $S_{\text{HA}}$ ) is given by Eq. (3), while its saturation index ( $SI$ ) is defined as Eq. (4) [59]:

$$S = a_A^a \times a_B^b \times a_C^c \times /K_{sp} \tag{2}$$

$$S_{\text{HA}} = \left( (a_{\text{Ca}^{2+}})^5 \times (a_{\text{PO}_4^{3-}})^3 \times (a_{\text{OH}^-}) \right) / K_{\text{spHA}} \tag{3}$$

$$SI_{HA} = \log(S_{HA}) \quad (4)$$

The control of supersaturation is critically prominent in hydrothermal condition to design HA crystals of the desired size, because it has a linear dependence with growth rate [72].

If  $SI < 0$  the solution is undersaturated, and the mineral will dissolve into the solution; if  $SI = 0$ , the process dissolution and precipitation are in equilibrium.

When  $SI > 0$  the solution is supersaturated, and the mineral will preferentially precipitate from the solution and grow. At positive and low  $SI$ , crystals can grow faster than their nucleation, resulting in a larger crystal formation; however, at higher  $SI$  crystal, nucleation prevails over crystal growth and smaller crystals are formed.

Some authors have shown that different morphologies ranging from rod-like, to plate-like to spherical HA nanoparticles could be obtained by varying the supersaturation values of the chemical reaction in hydrothermal conditions [31, 73].  $SI$  value can also define a two-dimensional or layer-by-layer growth ( $-\Delta G_{2D}$ ), in which two particles share a common crystallographic orientation and the growing interface can shift only transversely, leading the final structures to thin sheets and plate shaped. Alternatively,  $SI$  value can define a three-dimensional or continuous growth ( $-\Delta G_{3D}$ ) where the interfaces can move without constraint [74].

### 3.2 Calcium- and phosphate-based precursors

HA is usually formed in the  $Ca-PO_4-H_2O$  hydrothermal system through a reaction between starting precursors, which contain  $Ca^{2+}$  (preferentially salts) and  $PO_4^{3-}$  ions, respectively. Each combination between  $Ca^{2+}$  and  $PO_4^{3-}$  sources can be used to create a specific method for preparing HA. Both ionic sources are mainly chosen as salts, to avoid the competitive formation of other CaP phases at external pH range of HA stability; for example, the use of phosphoric acid as phosphate source could precipitate the brushite phase [75, 76].

The most common chemical reactants used for the hydrothermal synthesis of HA are shown in **Table 3**, where the column of  $Ca^{2+}$  sources is split into soluble or insoluble forms.

Various synthetic strategies to form HA crystals were developed, and the related processes can be classified into two main types, based on the nature of Ca-based precursors that can be soluble or insoluble.

The mechanism of these processes follows several steps, which are schematically illustrated in **Figures 3** and **4**. In both cases, the hydrothermal treatment begins after the mixing of the precursors (and any additives).

By using the soluble calcium sources (**Figure 3**), the first step is the mixing of all soluble precursors in supersaturated conditions, followed by rapid nucleation, up to the formation of small nuclei (step of reaction between ions). The subsequent steps in hydrothermal conditions are the continuous growth of the nuclei and increasing of nanoparticle dimension by Ostwald ripening or maturation to reduce the overall energy (step of hydrothermal treatment) [73, 95].

Compared to synthesis with soluble salts, the alternative way (**Figure 4**) provides for an initial step of mixing of the precursors, by immersing the insoluble calcium salt in a phosphate solution. Then a dissolution-recrystallization mechanism proceeds at the solution/calcium sources interface in hydrothermal condition, through continuous nucleation-growth-ripening steps.

Calcium material undergoes a slow and gradual dissolution at the nanoscale, followed by the reaction between calcium and phosphate ions and by the nucleation/precipitation of HA crystals on the surface of dissolving calcium precursor. This process is thermodynamically favored due to the lower solubility product of



$\text{Ca}^{2+}$ Soluble sources		$\text{PO}_4^{3-}$ Sources
$\text{Ca}(\text{CH}_3\text{COO})_2$	+	$\text{NaH}_2\text{PO}_4$ [61, 62];
$\text{CaCl}_2 \cdot 2\text{H}_2\text{O}$	+	$\text{K}_2\text{HPO}_4$ [48, 77]; $\text{NaH}_2\text{PO}_4$ [67]; $\text{Na}_2\text{HPO}_4$ [18, 34]; $(\text{NH}_4)_2\text{HPO}_4$ [78]; $\text{C}_8\text{H}_{10}\text{NO}_6\text{P}$ (PLP) [35]; $\text{Na}_5\text{P}_3\text{O}_{10}$ (STPP) [31]
$\text{Ca}(\text{NO}_3)_2 \cdot 4\text{H}_2\text{O}$	+	$\text{KH}_2\text{PO}_4$ [23]; $\text{K}_2\text{HPO}_4$ [47]; $\text{NaH}_2\text{PO}_4$ [58, 63]; $\text{Na}_2\text{HPO}_4$ [36, 64]; $\text{Na}_3\text{PO}_4$ [32, 37, 38]; $\text{NH}_4\text{H}_2\text{PO}_4$ [39, 65, 68]; $(\text{NH}_4)_2\text{HPO}_4$ [20, 29, 40–45, 49, 50, 54, 56, 59, 60, 66, 70, 79–83] $(\text{NH}_4)_2\text{HPO}_4 + \text{NH}_4\text{H}_2\text{PO}_4$ [71, 84]
$\text{Ca}^{2+}$ Insoluble sources		$\text{PO}_4^{3-}$ Sources
$\text{Ca}(\text{OH})_2$	+	$(\text{NH}_4)_2\text{HPO}_4$ [85, 86] $\text{CaHPO}_4 \cdot 2\text{H}_2\text{O}$ [51]
$\text{CaSO}_4$	+	$(\text{NH}_4)_2\text{HPO}_4$ [87, 88]
$\text{CaCO}_3$	+	$(\text{NH}_4)_2\text{HPO}_4$ [89]; $\text{CaHPO}_4$ [46]
$\text{CaCO}_3$ (3-D)	+	$\text{NH}_4\text{H}_2\text{PO}_4$ [90]; $(\text{NH}_4)_2\text{HPO}_4$ [25, 91–93]; $\text{Na}_3\text{PO}_4$ [28]; $\text{K}_2\text{HPO}_4$ [94] $(\text{NH}_4)_2\text{HPO}_4 + \text{NH}_4\text{H}_2\text{PO}_4$ [26]
$\beta\text{-TCP}$	+	$\text{CaHPO}_4 \cdot 2\text{H}_2\text{O}$ (insolub.) [53]

**Table 3.**  
Most popular precursors in the  $\text{Ca-PO}_4\text{-H}_2\text{O}$  hydrothermal system for HA production.

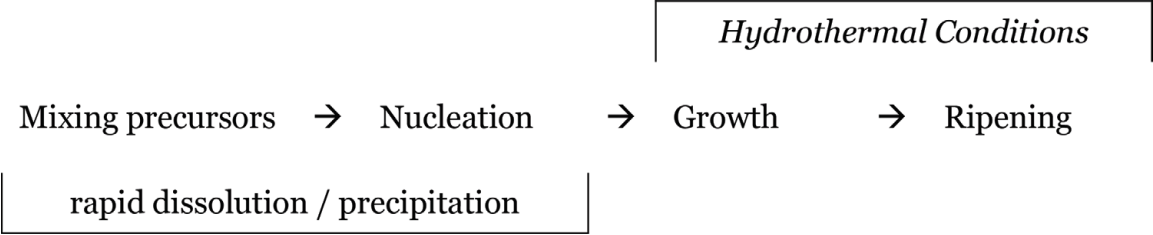


**Figure 3.**  
Synthesis scheme by using soluble calcium-based precursor (powder form).

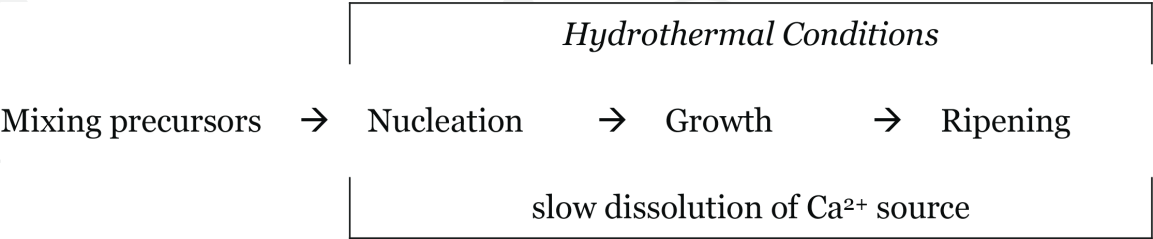


**Figure 4.**  
Synthesis scheme by using insoluble calcium-based precursor (powder or 3-D block forms).

HA compared to calcium sources ( $K_{\text{psHA}} \ll K_{\text{psCaCO}_3} < K_{\text{psCaSO}_4} < K_{\text{psCa}(\text{OH})_2}$ ). The solution where calcium source is soaked is initially undersaturated with respect to calcium; when source dissolves, it releases  $\text{Ca}^{2+}$ , and corresponding negative ions (e.g.,  $\text{CO}_3^{2-}$  or  $\text{OH}^-$ ) at the interface and a supersaturated condition, relating to HA, are created, and so it can start to precipitate and replace the original material.

The orientation of formed HA crystals may or may not have relationship with the parent calcium source crystal, with consequences on the structural control on the transformation from insoluble calcium source. But if calcium source has similar symmetry and unit cell dimensions of HA, the mineral replacement can

occur by an epitactic or topotactic growth of HA crystals on the surface of dissolving precursor crystals, so that its orientation determines the disposition of HA nanocrystals. This mechanism is particularly evident during the conversion process of biogenic source made of calcite, where  $\text{PO}_4^{3-}$  ions replace  $\text{CO}_3^{2-}$  at the interface to produce a 3-D structure of HA which accurately reproduces and preserves the whole complex morphology (external and internal) of the original calcite template [28]. Therefore, the greater versatility in tailoring of HA crystal size and morphology could be achieved through precipitation from homogeneous solutions containing both soluble calcium and phosphate sources. By adopting an insoluble salt of calcium as precursor, the degree of dissolution/precipitation, accompanied by interface reaction rate control, shall facilitate the formation of anisotropic particles which constitute the 3D structures.

### 3.3 Temperature

By shifting the dielectric constant and density with respect to temperature, water provides an excellent reaction medium for hydrothermal processing of HA nanostructured, leading to higher reaction rates and smaller particles than conventional processing route. According to the reaction temperature, hydrothermal synthesis can be classified into subcritical ( $T < 374^\circ\text{C}$ ) and supercritical ( $T > 374^\circ\text{C}$ ) synthesis, although these syntheses are typical subcritical, because they are easily applicable to industrial and laboratory operations. Subcritical conditions can be classified as mild (temperatures near to  $100^\circ\text{C}$ ) or elevated (temperature up to  $250^\circ\text{C}$ ). Many studies are done with synthesis temperature in the range from mild to elevated subcritical conditions ( $\sim 100\text{--}240^\circ\text{C}$ ), showing the formation of various morphologies of particles with different sizes [18, 19, 21, 37, 39, 48, 53, 55, 60, 80, 86, 87, 89].

Hydrothermal processes carried out at work temperature higher than  $250^\circ\text{C}$  are rarely documented in literature; for this purpose, rapid and continuous hydrothermal synthesis could be considered an appropriate technique [41, 80]. This could lead to the deterioration of the internal vessel (frequently made of inert polymer) or potential additives used during the process. Furthermore, high pressure and specific volume of water in the proximity to the supercritical point could damage the hydrothermal device. Anyway, the advantage of syntheses at very high temperature was not yet clearly evidenced in literature.

The synthesis temperature significantly affects the precipitation/dissolution of HA, and it is a crucial crystal growth parameter, because it regulates the supersaturation by means of solubility products  $K_{\text{ps}}$ , that is temperature dependent. The following equation (Eq. (5)) can express the solubility product of HA as a function of temperature [21, 96]:

$$\log K_{\text{spHA}} = -(a/T + bT + c) \quad (5)$$

where  $a$ ,  $b$ , and  $c$  are constant.

As a general rule, high temperature leads to the formation of large and long fibers/particles, while at low temperature small dimensions are preferred [12, 46, 81]. This depends on predominant growth, according to specific kinetic of crystallization and colloidal stability of particles [72].

Increasing hydrothermal temperature affects the significantly improving phase purity and Ca/P ratio of HA precipitate [93]. Crystallinity features are also affected by the change of synthesis temperature; an increased crystallinity with increased temperature occurs compared with those prepared at a low temperature because nuclei growth tends to happen at higher temperatures [18, 47].

Du et al. described the hydrothermal process through two transition temperatures to particle growth can be at 160°C and a temperature between 200 and 220°C: the first transition is for uniformity, where particles synthesized at temperatures above it are more uniform, while the second limits the expansion of the particle length [97].

### 3.4 pH: phosphate equilibrium

pH is an important parameter that can be modified from alkaline to acidic condition to obtain the desired morphology of HA nanostructures.

pH condition performs the synthesis through two different ways: (i) by affecting the distribution of phosphate species in solution, according to the distribution of phosphate species ( $\text{H}_3\text{PO}_4$ ,  $\text{H}_2\text{PO}_4^-$ ,  $\text{HPO}_4^{2-}$ , and  $\text{PO}_4^{3-}$ ) against the pH value, as well as (ii) the modification of the electrical charge on the HA crystal surface.

- i. Different calcium phosphate intermediates are formed by adjusting the pH value; among them, the precipitation of HA may occur preferentially from slightly acidic condition up to basic pH conditions (approximately in the range of 5–11). Therefore, the solubility (or instability) of HA is highly affected under acidic conditions and decreases with increasing pH. The solubility isotherms of the CaP phases as a function of pH value and calcium (or phosphate) concentration from room temperature to hydrothermal conditions (e.g.,  $T = 200^\circ\text{C}$ ) are shown in **Figure 5**. At  $25^\circ\text{C}$  the HA stability field exists at equilibrium  $\text{pH} > 4.8$  (**Figure 5a**), whereas at  $200^\circ\text{C}$  the HA stability field extends to an equilibrium pH as low as 2.9 (**Figure 5b**).

An increment of pH value shifts the phosphate species equilibrium from  $\text{H}_3\text{PO}_4 \rightarrow \text{H}_2\text{PO}_4^- \rightarrow \text{HPO}_4^{2-} \rightarrow \text{PO}_4^{3-}$ , respectively, and increase the saturation index of HA according to Eq. (6) [74]:

$$\log \text{SI}_{\text{HA}} = 4 \text{ pH} - 72.08 \quad (6)$$

This means that at  $\text{pH} \sim 5$  the  $\text{SI} = 1$ , while at higher pH the solution, is supersaturated and at lower pH is undersaturated. In other words, an increase in pH from about 5 results in increases in the nucleation rate of HA and its subsequent crystal growth.

- ii. The pH affects the electric charge of the HA crystal surface by changing the distribution of hydroxyl groups or protons. It was experimentally estimated that the zero charge point for HA in solutions occurs close to neutral pH, for which, in basic or acidic conditions, the crystal surface will be negatively or positively charged, as result of preferred absorption of  $\text{Ca}^{2+}$  and  $\text{PO}_4^{3-}$  ions on the a-axis or c-axis; pH value results in anisotropic growth of the crystallites that will be into one-dimensional nanorods or two-dimensional nanoplates.

Alkaline conditions produce smaller and less elongated particles at any certain orientation, while the formation of rod-like or needle-like and c-axis elongated HA particles with hydrothermal process occurs at acidic conditions [20, 42, 43]. The variation in acidic pH has a pronounced influence on the length of the rod-like particles, due to the protonation trend of the a-axis.

More complex HA particles, including three-dimensional feathery, microfiber, and microcube structures were obtained by modulating pH during the synthesis [13].

In addition to temperature, the degree of crystallinity of final HA is also affected by difference in pH that can modify the nucleation and growth rates of the nuclei [42]; for example, higher crystallinity was observed in samples that were prepared at low pH conditions [8, 13].

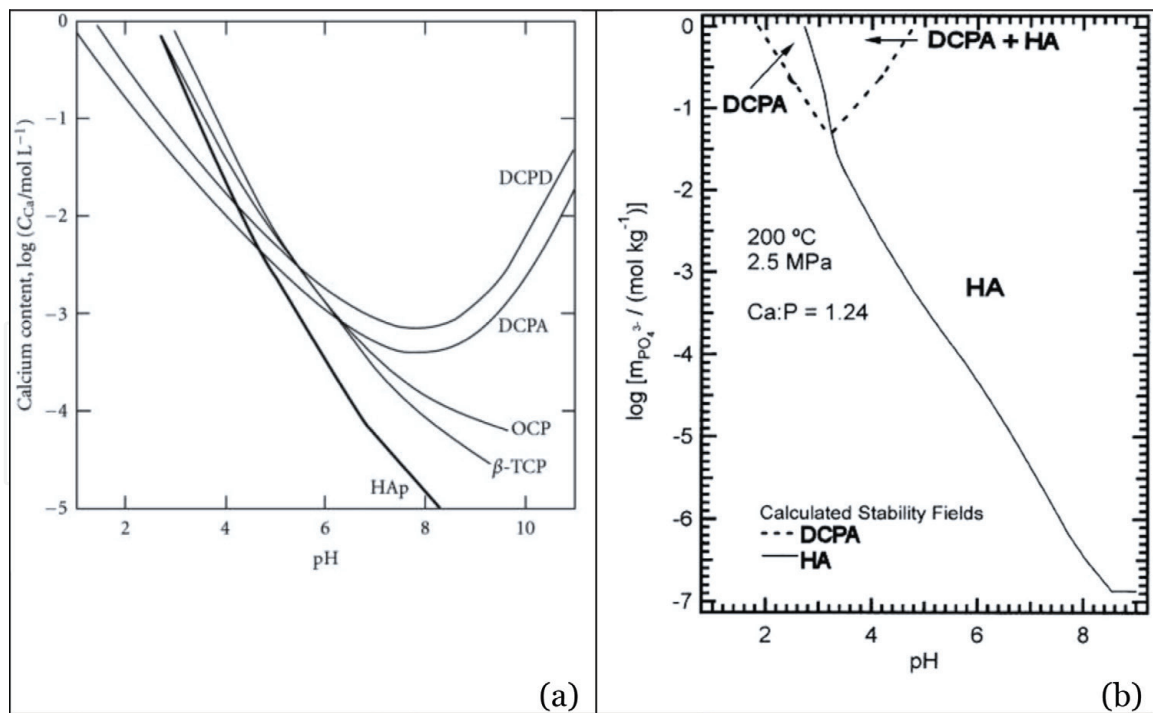


**Figure 5.** Diagrams for the  $\text{Ca-PO}_4\text{-H}_2\text{O}$  system at 25°C (a) and 200°C (b) as a function of the equilibrium solution pH.

Sadat-Shojai et al. have recently reported that HA nanorods having high crystallinity and high aspect ratio could merely be prepared through precipitation at approximately neutral conditions followed by hydrothermal treatment at 200°C for 60 h. In this case, the nanoparticles show high dispersion stability, indicating their high surface charge and a low tendency for agglomeration [98].

The aspect ratio of HA particles is significantly affected by the pH of the reaction mixture; the mean aspect ratio of nanoparticles greatly decreases with increasing pH.

### 3.5 Process time

Process time, if prolonging, would enlarge the size of HA particles and also contribute to increasing the crystallinity. Its less significant factor affects the structural and morphological characteristics of HA nanoparticles, if compared with temperature and pH.

As temperature and pH affect the dissolution of HA, by maintaining these conditions as constants, it can be seen that this HA property is determined as a function of time. The concentration in hydrothermal solution of ionic species constituting HA is in relationship with process time, in accordance with classical parabolic behavior, expressed by Eq. (7),

$$[C]^2 = Kt + A \approx Kt \quad (7)$$

where  $[C]$  is the concentration of ions,  $A$  is a constant,  $K$  is the parabolic rate constant, and  $t$  is the process time. For various hydrothermal temperature, a dissolution equilibrium time up to the achievement of plateau could be reached.

This equilibrium time of the reactions would be shortened with the increasing of hydrothermal temperature. For example, at neutral pH, Zhang et al. had observed an equilibrium time after 10 h at 300°C and after 12 h at 200°C [96].

Several studies report the linear increasing of the synthesized length of HA nanoparticles up to a synthesis time limit. At 150 and 200°C, respectively, Jin et al. and Earl et al. observed the elongation of nanorods within 24 h; for the range of



24–72 hours of synthesis, crystallinity and size are not significantly affected by the differences in synthesis duration [20, 37].

Over the equilibrium time, self-assembly phenomena can occur toward more complex forms, i.e., flower-like morphologies [68], while in 3-D biomorphic conversion, prolonged heating time could influence the aggregation and morphology of HA through a rearrangement of the building blocks such as nanosheets and nanorods.

Hydrothermal treatment can be done in various time-temperature profiles designed as serious, stepwise, slow, intervallic thermal heating, etc. By carefully changing these profiles, the final morphologies of the resulting powder can be plates, hexagonal prisms, needles, and fine-plates, respectively [29].

The prolonged time can affect the colloidal stability and decomposition of any additives that will further be discussed in Section 3.7.

### 3.6 Concentration/ion ratio

The final HA morphologies are sensitive to the concentration of ions during the reaction, defining the degree of supersaturation (Eqs. (2) and (3)).

Depending only by the concentration of the precursors, the HA nanostructures can form different morphologies. Hao et al. have observed that HA particles could have irregular or uniform plate-like forms, which tend to aggregate into small fibrous bundles, by increasing calcium concentration in solution [59].

Some authors claim that the diameter of the particles increases with the increment of reactant concentration because less concentrated chemical material limits the ion transportation. The increments of the mean length of the particles are also concluded to be significantly affected by the concentration of the initial material [42].

It is known that HA powders can be prepared with controlled Ca/P molar ratio (stoichiometric value is 1.67) in accordance to the starting amount of  $\text{Ca}^{2+}$  and  $\text{PO}_4^{3-}$  in solution [29, 98]. If the starting calcium precursor is  $\text{CaCO}_3$ , the resulting HA products will be not stoichiometric, due to partial substitutions of the anions ( $\text{PO}_4^{3-}$ , and  $\text{OH}^-$ ) by  $\text{CO}_3^{2-}$  groups.

### 3.7 Additives

Recently, it was found that additional components are usually included with the precursors to modify the morphology and size of the produced HA nanostructures, during hydrothermal synthesis. Some of the most popular additives used in many hydrothermal syntheses are listed in **Table 4** and classified on the basis of their chemical characteristic. They include organic or inorganic matrices.

The intrinsically different surface reactivity of HA crystals (positively charged  $\text{Ca}^{2+}$ -rich c-surface and negatively charged  $\text{OH}^-$ - and  $\text{PO}_4^{3-}$ -rich a-surface) can selectively adsorb various ions, organic compounds, and proteins.

Long HA whiskers can be prepared by homogeneous hydrothermal precipitation using acetamide, as a result of hydrolysis at elevated temperature and following interaction between acetic ions with their negative charges and the a-sites of HA [60]. This match also characterizes citrate salts [38].

Urea influences the increase of the diameter of HA nanoparticles because its hydrolysis introduces  $\text{CO}_3^{2-}$  ions, incorporated inside the HA crystal structure; therefore, it controls the pH value through  $\text{NH}_3$  release, affecting the nucleation and growth of HA crystals. Intensive decomposition of urea increases supersaturation and subsequently produces more nuclei and smaller crystals [42].

Chelating agent (e.g. EDTA or tartrate) can induce the formation of a ring-like structure through the complex with  $\text{Ca}^{2+}$  contained in HA. Final particles can be obtained after decomposition of these structures in controlled hydrothermal treatment.

Properties	Additive
Electrolytes	Acetamide (AA) [60], urea [29, 42, 58, 68], Na-citrate [37, 38, 44], propionamide (PA) [59], etc.
Chelating agents	Ethylenediaminetetraacetic acid (EDTA) [36], K-Na-tartrate [67], etc.
Organic modifiers/surfactants	Cetyltrimethylammonium bromide (CTAB) [77, 99], glutamic acid (Glu) [31, 66], liposome [83], polyethylene glycol (PEG) [43], polyvinylpyrrolidone (PVP) [39], macromolecule (HTCC) [33], etc.
Proteins	Hemoglobin [62], lysine (Ly) [56], etc.

**Table 4.**  
*Various additives commonly used during hydrothermal synthesis of calcium phosphate.*

As a result of complexation, the concentration of free calcium ions dramatically decreases, leading to the HA nuclei with smaller size and quantity. During the hydrothermal treatment, calcium ions are released, and each nucleus will grow to the distinct single needle-like particles and finally to well-separated long fibers. It is well known that increasing pH value has a considerable improvement on complexes stability. The subsequent hydrothermal treatment leads to the Ca-complex decomposition and HA crystals are grown on the previously formed pattern, according to anisotropic growth along the c-axis.

Surfactants are usually used as the controlling reagent to prepare 3-D architecture of HA-based materials. Contrary to anionic reactant like EDTA, the cationic surfactant CTAB can bind with  $\text{PO}_4^{3-}$  of reaction system by the ionic charge and stereochemistry due to their complementarity tetrahedral structures, so that phosphate anion can be incorporated to the formed nuclei, and the final HA and size of HA particles can be well controlled. During the hydrothermal process, CTAB-HA complexes are created, and their controlled coalescence produce nanorods with uniform morphology and controllable size [99].

Some attempts have been made to exploit the developed organic materials in controlling the crystal growth of HA. Zhu et al. [33] synthesized rod-like HA nanoparticles of various aspect ratios by means of the hydrothermal method in the presence of HTCC as a cationic polymer template. HTCC molecules are first incorporated into  $\text{PO}_4^{3-}$  and  $\text{OH}^-$  anions by charge and stereochemical complementarity, and the rigid chains of polymer molecules are then converted to extended chains, connected through the ion bonds of  $\text{PO}_4^{3-}$  to form a 2D structure, followed by formation of a 3D rod-like morphology through self-assembling process via hydrogen bond interactions. Nucleation and subsequent crystal growth can occur upon adding the Ca precursor and hydrothermal treatment, respectively.

Recently, a novel hydrothermal method based on the liquid-solid-solution strategy has been developed to synthesize surface-modified HA nanorods of various aspect ratios. According to this strategy, controlled growth of HA nanorods with tunable morphology can be achieved by adequately tuning the interfaces between surfactants and the central atoms of HA. Nanostructured HA with desired characteristics can be fabricated by using organic modifiers, such as PEG, Tween-20, sorbitol, etc., in various hydrothermal conditions. For example, they favor the formation of HA nanorods with a larger aspect ratio, or small-sized, or long length, respectively, at high or low synthesis temperature.

Some proteins have an affinity to a specific face of HA crystals, and they are strong inhibitors for perpendicular growth to the adsorbed face, in hydrothermal conditions at low temperature. For example, if the c-plane is covered by proteins

(e.g., hemoglobin molecules), the crystal will preferentially grow in the direction of the a-axis to form HA nanosheets. Then the hemoglobin could adsorb on the surface of newly formed HA nanosheets to increase their dimension. At high temperature, the hemoglobin could be hydrolyzed and decomposed under the hydrothermal conditions, and the degraded products could be differently adsorbed by the formed HA nanosheets up to the formation of different structures (e.g., flower-like or dandelion-like morphologies) [62].

4. Conclusions

The hydrothermal method is particularly appropriate for the realization of good-quality crystals and allows tailored HA nanosized particles to be synthesized or characteristic of 3-D structures.

This chapter discussed about the most influencing variables in the hydrothermal synthesis of HA and their effects to prepare a wide range of crystal morphologies.

Among the considered variables, temperature and pH seem to be the most significant factors affecting the dimensional, geometry, and crystalline characteristics of HA nanoparticles, e.g., through face-selective interaction and anisotropic growth processes.

**Table 5** summarizes the process parameters discussed and their effects and contribution on the final structures, which can have the form of hexagonal prisms (rods, needles, wires), sheets, plates, whiskers, fine spherical-shaped, etc., of varying sizes.

This extensive range of morphologies may be useful for developing various and improved types of nanostructured biomaterials, which could have potential application for repairing bone defects and tissue regeneration.

Conditions	Effects	Low values	High values
Supersaturation	Crystal size, size distribution	Large particles, 2D growth	Small particles, 3D growth
Selection of precursors	HA precipitation, crystals orientation	—	—
Concentration	Saturation, Ca/P molar ratio control	—	Increase particle dimension
Temperature	Solubility, nucleation, growth	Small particles, low crystallinity	Large particles, high phase purity, high crystallinity
pH	Crystal growth rate, anisotropic growth of crystals	Small particles, preferential growth along c-axis (rod shape), high crystallinity	Large particles, preferential growth along a-axis (plate shape)
Process time	Ripening	Small size	Large size, high crystallinity
Additives	Structures control, complex geometry	Various effects	Various effects

**Table 5.**  
*Summary scheme of the hydrothermal parameters contribution on the final HA nanostructure.*

## Conflict of interest

The authors declare no conflict of interest.

IntechOpen

IntechOpen

## Author details

Andrea Ruffini\*, Simone Sprio, Lorenzo Preti and Anna Tampieri  
CNR-ISTEC – Institute of Science and Technology for Ceramics, Faenza, RA, Italy

\*Address all correspondence to: [andrea.ruffini@istec.cnr.it](mailto:andrea.ruffini@istec.cnr.it)

## IntechOpen

© 2019 The Author(s). Licensee IntechOpen. This chapter is distributed under the terms of the Creative Commons Attribution License (<http://creativecommons.org/licenses/by/3.0>), which permits unrestricted use, distribution, and reproduction in any medium, provided the original work is properly cited. 



## References

- [1] Bohner M. Calcium orthophosphates in medicine: From ceramics to calcium phosphate cements. *Injury*. 2000;**31**:D37-D47
- [2] Sprio S, Sandri M, Ruffini A, Adamiano A, Iafisco M, Dapporto M, et al. Tissue engineering and biomimetics with bioceramics. In: *Advances in Ceramic Biomaterials*. Elsevier, Ltd., Woodhead Publishing; 2017. pp. 407-432
- [3] He W, Andersson M. Biomimetic synthesis of nanostructured calcium phosphates. In: *Frontiers in Nanobiomedical Research*. Singapore: The World Scientific Encyclopedia of Nanomedicine and Bioengineering II. 2017. pp. 85-124
- [4] Kumta PN, Sfeir C, Lee D-H, Olton D, Choi D. Nanostructured calcium phosphates for biomedical applications: Novel synthesis and characterization. *Acta Biomaterialia*. 2005;**1**(1):65-83
- [5] Hui P, Meena SL, Singh G, Agarawal RD, Prakash S. Synthesis of hydroxyapatite bio-ceramic powder by hydrothermal method. *Journal of Minerals and Materials Characterization and Engineering*. 2010;**09**(08):683-692
- [6] Weiner S, Traub W, Wagner HD. Lamellar bone: Structure–function relations. *Journal of Structural Biology*. 1999;**126**(3):241-255
- [7] Lee J-W, Yun H-S, Nakano T. Induction of biological apatite orientation as a bone quality parameter in bone regeneration using hydroxyapatite/poly caprolactone composite scaffolds. *Tissue Engineering. Part C, Methods*. 2016;**22**(9):856-863
- [8] Liu Q, Huang S, Matinlinna JP, Chen Z, Pan H. Insight into biological apatite: Physiochemical properties and preparation approaches. *BioMed Research International*. 2013;**2013**:1-13
- [9] Ferraz MP, Monteiro FJ, Manuel CM. Hydroxyapatite nanoparticles: A review of preparation methodologies. *Journal of Applied Biomaterials & Biomechanics*. 2004;**2**(2):74-80
- [10] Fatimah M, Shaaban ASA, Seliman SSS. Overview: Process parameters for hydrothermal synthesis of hydroxyapatite. *Journal of Advanced Manufacturing Technology*. 2012;**6**(1):47-59
- [11] Chen F, Zhu Y, Wu J, Huang P, Cui D. Nanostructured calcium phosphates: Preparation and their application in biomedicine. *Nano Biomedicine and Engineering*. 2012;**4**(1):41-49
- [12] Loo SCJ, Siew YE, Ho S, Boey FYC, Ma J. Synthesis and hydrothermal treatment of nanostructured hydroxyapatite of controllable sizes. *Journal of Materials Science. Materials in Medicine*. 2008;**19**(3):1389-1397
- [13] Sadat-Shojai M, Khorasani M-T, Dinpanah-Khoshdargi E, Jamshidi A. Synthesis methods for nanosized hydroxyapatite with diverse structures. *Acta Biomaterialia*. 2013;**9**(8):7591-7621
- [14] Dorozhkin SV, Epple M. Biological and medical significance of calcium phosphates. *Angewandte Chemie, International Edition*. 2002;**41**(17):3130-3146
- [15] Wang L, Nancollas GH. Calcium orthophosphates: Crystallization and dissolution. *Chemical Reviews*. 2008;**108**(11):4628-4669
- [16] Okada M, Matsumoto T. Synthesis and modification of apatite nanoparticles for use in dental and medical applications. *Japanese Dental Science Review*. 2015;**51**(4):85-95
- [17] Iwamoto T, Hieda Y, Kogai Y. Effect of hydroxyapatite surface morphology

on cell adhesion. *Materials Science and Engineering: C*. 2016;**69**:1263-1267

[18] Li R, Cai Y, Yang Y, Fang S, Su X, Sun Y, et al. Dimensionally and morphologically controlled growth of calcium phosphate crystals by an organic-free hydrothermal process. *Ceramics International*. 2016;**42**(15):17387-17397

[19] Mohan N, Palangadan R, Varma H. Hydroxyapatite scaffolds constituting highly oriented crystals derived from synthetic precursors by hydrothermal reactions. *Ceramics International*. 2016;**42**(15):17259-17268

[20] Earl JS, Wood DJ, Milne SJ. Hydrothermal synthesis of hydroxyapatite. *Journal of Physics Conference Series*. 2006;**26**:268-271

[21] Byrappa K, Adschiri T. Hydrothermal technology for nanotechnology. *Progress in Crystal Growth and Characterization of Materials*. 2007;**53**(2):117-166

[22] Yoshimura M, Sujaridworakun P, Koh F, Fujiwara T, Pongkao D, Ahniyaz A. Hydrothermal conversion of calcite crystals to hydroxyapatite. *Materials Science and Engineering: C*. 2004;**24**(4):521-525

[23] Ashok M, Kalkura SN, Sundaram NM, Arivuoli D. Growth and characterization of hydroxyapatite crystals by hydrothermal method. *Journal of Materials Science: Materials in Medicine*. 2007;**18**(5):895-898

[24] Hiroaki O, Shin Y. Hydrothermal synthesis of calcium phosphate from Corbicula shells. *Journal of Ecotechnology Research*. 2016;**18**(1):7-10

[25] Vecchio KS, Zhang X, Massie JB, Wang M, Kim CW. Conversion of

bulk seashells to biocompatible hydroxyapatite for bone implants. *Acta Biomaterialia*. 2007;**3**(6):910-918

[26] Ruffini A, Sprio S, Tampieri A. Study of the hydrothermal transformation of wood-derived calcium carbonate into 3D hierarchically organized hydroxyapatite. *Chemical Engineering Journal*. 2013;**217**:150-158

[27] Jinawath S, Polchai D, Yoshimura M. Low-temperature, hydrothermal transformation of aragonite to hydroxyapatite. *Materials Science and Engineering: C*. 2002;**22**(1):35-39

[28] Álvarez-Lloret P, Rodríguez-Navarro AB, Falini G, Fermani S, Ortega-Huertas M. Crystallographic control of the hydrothermal conversion of calcitic Sea urchin spine (*paracentrotus lividus*) into apatite. *Crystal Growth & Design*. 2010;**10**(12):5227-5232

[29] Neira IS, Kolen'ko YV, Lebedev OI, Van Tendeloo G, Gupta HS, Guitián F, et al. An effective morphology control of hydroxyapatite crystals via hydrothermal synthesis. *Crystal Growth & Design*. 2009;**9**(1):466-474

[30] Jinawath S, Pongkao D, Suchanek W, Yoshimura M. Hydrothermal synthesis of monetite and hydroxyapatite from monocalcium phosphate monohydrate. *International Journal of Inorganic Materials*. 2001;**3**(7):997-1001

[31] Yang Y, Wu Q, Wang M, Long J, Mao Z, Chen X. Hydrothermal synthesis of hydroxyapatite with different morphologies: Influence of supersaturation of the reaction system. *Crystal Growth & Design*. 2014;**14**(9):4864-4871

[32] Su J, Liang, Yunfei, Shuhua, Song, Zhuojing. Effects of hydrothermal treatment on the properties of

nanoapatite crystals. *International Journal of Nanomedicine*. 2012;**7**:5151-5158

[33] Zhu A, Lu Y, Si Y, Dai S. Fabricating hydroxyapatite nanorods using a biomacromolecule template. *Applied Surface Science*. 2011;**257**(8):3174-3179

[34] Lim H, Kassim A, Ming H. Preparation and characterization of calcium phosphate nanorods using reverse microemulsion and hydrothermal processing routes. *Sains Malaysiana*. 2010;**39**:267-273

[35] Zhao X-Y, Zhu Y-J, Lu B-Q, Chen F, Qi C, Zhao J, et al. Hydrothermal synthesis of hydroxyapatite nanorods using pyridoxal-5'-phosphate as a phosphorus source. *Materials Research Bulletin*. 2014;**55**:67-70

[36] Xin R, Ren F, Leng Y. Synthesis and characterization of nano-crystalline calcium phosphates with EDTA-assisted hydrothermal method. *Materials and Design*. 2010;**31**(4):1691-1694

[37] Jin X, Chen X, Cheng Y, Wang L, Hu B, Tan J. Effects of hydrothermal temperature and time on hydrothermal synthesis of colloidal hydroxyapatite nanorods in the presence of sodium citrate. *Journal of Colloid and Interface Science*. 2015;**450**:151-158

[38] Jin X, Zhuang J, Zhang Z, Guo H, Tan J. Hydrothermal synthesis of hydroxyapatite nanorods in the presence of sodium citrate and its aqueous colloidal stability evaluation in neutral pH. *Journal of Colloid and Interface Science*. 2015;**443**:125-130

[39] Hu J, Zhou Y, Huang L, Liu J, Lu H. Effect of nano-hydroxyapatite coating on the osteoinductivity of porous biphasic calcium phosphate ceramics. *BMC Musculoskeletal Disorders*. 2014;**15**(1):1-11

[40] Buitrago-Vásquez M, Ossa-Orozco CP. Hydrothermal synthesis of hydroxyapatite nanorods using a fruit extract template. *DYNA*. 2018;**85**(204):283-288

[41] Chaudhry AA, Haque S, Kellici S, Boldrin P, Rehman I, Khalid FA, et al. Instant nano-hydroxyapatite: A continuous and rapid hydrothermal synthesis. *Chemical Communications*. 2006;**21**:2286-2288

[42] Sadat-Shojai M, Atai M, Nodehi A. Design of experiments (DOE) for the optimization of hydrothermal synthesis of hydroxyapatite nanoparticles. *Journal of the Brazilian Chemical Society*. 2011;**22**(3):571-582

[43] Salariana M, Solati-Hashjin M, Goudarzi A, Shafiei SS, Salarian R, Nemati ZA. Effect of surfactant in formation of hydroxyapatite Nano-rods under hydrothermal conditions. *Iranian Journal of Pharmaceutical Sciences*. 2008;**4**(2):157-162

[44] Yang H, Zeng H, Hao L, Zhao N, Du C, Liao H, et al. Effects of hydroxyapatite microparticle morphology on bone mesenchymal stem cell behavior. *Journal of Materials Chemistry B*. 2014;**2**(29):4703-4710

[45] Yubao L, De Wijn J, Klein CPAT, Van De Meer S, De Groot K. Preparation and characterization of nanograde osteoapatite-like rod crystals. *Journal of Materials Science. Materials in Medicine*. 1994;**5**(5):252-255

[46] Zhang X, Vecchio KS. Hydrothermal synthesis of hydroxyapatite rods. *Journal of Crystal Growth*. 2007;**308**(1):133-140

[47] Méndez-Lozano N, Velázquez-Castillo R, Rivera-Muñoz EM, Bucio-Galindo L, Mondragón-Galicia G, Manzano-Ramírez A, et al. Crystal growth and structural analysis of hydroxyapatite nanofibers



synthesized by the hydrothermal microwave-assisted method. *Ceramics International*. 2017;**43**(1):451-457

and the effect on mesenchymal stem cell behavior. *Ceramics International*. 2017;**43**(1):1588-1596

[48] Ban S, Hasegawa J. Morphological regulation and crystal growth of hydrothermal-electrochemically deposited apatite. *Biomaterials*. 2002;**23**(14):2965-2972

[55] Lin K, Chang J, Liu X, Chen L, Zhou Y. Synthesis of element-substituted hydroxyapatite with controllable morphology and chemical composition using calcium silicate as precursor. *CrystEngComm*. 2011;**13**(15):4850

[49] Chen C, Huang Z, Yuan W, Li J, Cheng X, Chi R. Pressure effecting on morphology of hydroxyapatite crystals in homogeneous system. *CrystEngComm*. 2011;**13**(5):1632-1637

[56] Chen YQ, Xing XF, Gao WM. Synthesis of spherical nano-hydroxyapatite by hydrothermal method with L-lysine template. *Key Engineering Materials*. 2014;**633**:17-20

[50] Yubao L, De Groot K, De Wijn J, Klein CPAT, Meer SVD. Morphology and composition of nanograde calcium phosphate needle-like crystals formed by simple hydrothermal treatment. *Journal of Materials Science. Materials in Medicine*. 1994;**5**(6-7):326-331

[57] Costa DO, Dixon SJ, Rizkalla AS. One- and three-dimensional growth of hydroxyapatite nanowires during sol-gel-hydrothermal synthesis. *ACS Applied Materials & Interfaces*. 2012;**4**(3):1490-1499

[51] Goto T, Kamitakahara M, Kim IY, Ohtsuki C. Effects of ethanol addition on formation of hydroxyapatite through hydrothermal treatment of dicalcium phosphate dihydrate. *IOP Conference Series: Materials Science and Engineering*. 2011;**18**(19):192015

[58] Jokić B, Mitrić M, Radmilović V, Drmanić S, Petrović R, Janačković D. Synthesis and characterization of monetite and hydroxyapatite whiskers obtained by a hydrothermal method. *Ceramics International*. 2011;**37**(1):167-173

[52] Han Y, Xu K, Montay G, Fu T, Lu J. Evaluation of nanostructured carbonated hydroxyapatite coatings formed by a hybrid process of plasma spraying and hydrothermal synthesis. *Journal of Biomedical Materials Research*. 2002;**60**(4):511-516

[59] Hao L, Yang H, Zhao N, Du C, Wang Y. Controlled growth of hydroxyapatite fibers precipitated by propionamide through hydrothermal synthesis. *Powder Technology*. 2014;**253**:172-177

[53] Watanabe T, Kawachi G, Kamitakahara M, Kikuta K, Ohtsuki C. Formation of needle-like hydroxyapatite by hydrothermal treatment of  $\text{CaHPO}_4 \cdot 2\text{H}_2\text{O}$  combined with  $\beta\text{-Ca}_3(\text{PO}_4)_2$ . *Journal of the Ceramic Society of Japan*. 2009;**117**(1366):759-764

[60] Zhang H, Darvell BW. Formation of hydroxyapatite whiskers by hydrothermal homogeneous precipitation using acetamide: Formation of hydroxyapatite whiskers. *Journal of the American Ceramic Society*. 2011;**94**(7):2007-2013

[54] Xiao D, Guo T, Yang F, Feng G, Shi F, Li J, et al. In situ formation of nanostructured calcium phosphate coatings on porous hydroxyapatite scaffolds using a hydrothermal method

[61] Zhao X-Y, Zhu Y-J, Chen F, Lu B-Q, Wu J. Nanosheet-assembled hierarchical nanostructures of hydroxyapatite: Surfactant-free microwave-hydrothermal rapid synthesis, protein/DNA adsorption and pH-controlled release. *CrystEngComm*. 2013;**15**(1):206-212



- [62] Zhao X-Y, Zhu Y-J, Zhao J, Lu B-Q, Chen F, Qi C, et al. Hydroxyapatite nanosheet-assembled microspheres: Hemoglobin-templated synthesis and adsorption for heavy metal ions. *Journal of Colloid and Interface Science*. 2014;**416**:11-18
- [63] Guan J-J, Tian B, Tang S, Ke Q-F, Zhang C-Q, Zhu Z-A, et al. Hydroxyapatite coatings with oriented nanoplate arrays: Synthesis, formation mechanism and cytocompatibility. *Journal of Materials Chemistry B*. 2015;**3**(8):1655-1666
- [64] Zhang H, Zhou K, Li Z, Huang S. Plate-like hydroxyapatite nanoparticles synthesized by the hydrothermal method. *Journal of Physics and Chemistry of Solids*. 2009;**70**(1):243-248
- [65] Lin K, Zhou Y, Zhou Y, Qu H, Chen F, Zhu Y, et al. Biomimetic hydroxyapatite porous microspheres with co-substituted essential trace elements: Surfactant-free hydrothermal synthesis, enhanced degradation and drug release. *Journal of Materials Chemistry*. 2011;**21**(41):16558
- [66] Qi M, Qi J, Xiao G, Zhang K, Lu C, Lu Y. One-step hydrothermal synthesis of carbonated hydroxyapatite porous microspheres with a large and uniform size regulated by l-glutamic acid. *CrystEngComm*. 2016;**18**(31):5876-5884
- [67] Ma M-G. Hierarchically nanostructured hydroxyapatite: Hydrothermal synthesis, morphology control, growth mechanism, and biological activity. *International Journal of Nanomedicine*. 2012;**7**:1781-1791
- [68] Lin K, Chang J, Zhu Y, Wu W, Cheng G, Zeng Y, et al. A facile one-step surfactant-free and low-temperature hydrothermal method to prepare uniform 3D structured carbonated apatite flowers. *Crystal Growth & Design*. 2009;**9**(1):177-181
- [69] Aldrich DS, Smith MA. Pharmaceutical applications of infrared microspectroscopy. *Applied Spectroscopy Reviews*. 1999;**34**(4):275-327
- [70] Neira IS, Guitián F, Taniguchi T, Watanabe T, Yoshimura M. Hydrothermal synthesis of hydroxyapatite whiskers with sharp faceted hexagonal morphology. *Journal of Materials Science*. 2008;**43**(7):2171-2178
- [71] Riman R. Solution synthesis of hydroxyapatite designer particulates. *Solid State Ionics*. 2002;**151**(1-4):393-402
- [72] Koutsopoulos S. Kinetic study on the crystal growth of hydroxyapatite. *Langmuir*. 2001;**17**(26):8092-8097
- [73] Pang YX, Bao X. Influence of temperature, ripening time and calcination on the morphology and crystallinity of hydroxyapatite nanoparticles. *Journal of the European Ceramic Society*. 2003;**23**(10):1697-1704
- [74] Viswanath B, Ravishankar N. Controlled synthesis of plate-shaped hydroxyapatite and implications for the morphology of the apatite phase in bone. *Biomaterials*. 2008;**29**(36):4855-4863
- [75] Onoda H, Yamazaki S. Homogenous hydrothermal synthesis of calcium phosphate with calcium carbonate and corbicula shells. *Journal of Asian Ceramic Societies*. 2016;**4**(4):403-406
- [76] Prakash KH, Kumar R, Ooi CP, Cheang P, Khor KA. Apparent solubility of hydroxyapatite in aqueous medium and its influence on the morphology of nanocrystallites with precipitation temperature. *Langmuir*. 2006;**22**(26):11002-11008
- [77] Wang Y, Zhang S, Wei K, Zhao N, Chen J, Wang X. Hydrothermal synthesis of hydroxyapatite

nanopowders using cationic surfactant as a template. *Materials Letters*. 2006;**60**(12):1484-1487

[78] Manoj M, Subbiah R, Mangalaraj D, Ponpandian N, Viswanathan C, Park K. Influence of growth parameters on the formation of hydroxyapatite (HAp) nanostructures and their cell viability studies. *Nano*. 2015;**2**:2

[79] Rafique MMA. Hydrothermal processing of phase pure and doped hydroxyapatite and its characterization. *Journal of Encapsulation and Adsorption Sciences*. 2018;**08**(01):18-37

[80] Chaudhry AA, Knowles JC, Rehman I, Darr JA. Rapid hydrothermal flow synthesis and characterisation of carbonate- and silicate-substituted calcium phosphates. *Journal of Biomaterials Applications*. 2013;**28**(3):448-461

[81] Jiang D, Zhang J. Calcium phosphate with well controlled nanostructure for tissue engineering. *Current Applied Physics*. 2009;**9**(3):S252-S256

[82] Nagata F, Yamauchi Y, Tomita M, Kato K. Hydrothermal synthesis of hydroxyapatite nanoparticles and their protein adsorption behavior. *Journal of the Ceramic Society of Japan*. 2013;**121**(1417):797-801

[83] Ramedani A, Yazdanpanah A, Moztafzadeh F, Mozafari M. On the use of nanoliposomes as soft templates for controlled nucleation and growth of hydroxyapatite nanocrystals under hydrothermal conditions. *Ceramics International*. 2014;**40**(7):9377-9381

[84] Vecbiskena L, de Nardo L, Chiesa R. Nanostructured calcium phosphates for biomedical applications. *Key Engineering Materials*. 2014;**604**:212-215

[85] Jokačević V, Izvonač D, Damićanin MD, Jokačević B, Živojinović V,

Marković D, et al. Hydrothermal synthesis and nanostructure of carbonated calcium hydroxyapatite. *Journal of Materials Science: Materials in Medicine*. 2006;**17**(6):539-546

[86] Ortiz SL, Avila JH, Gutierrez MP, Gómez-Pozos H, Karthik TVK, Lugo VR. Hydrothermal synthesis and characterization of hydroxyapatite microstructures. In: 14th International Conference on Electrical Engineering, Computing Science and Automatic Control (CCE). IEEE Xplore Digital online. 2017. pp. 1-4

[87] Bingöl OR, Durucan C. Hydrothermal synthesis of hydroxyapatite from calcium Sulfate hemihydrate. *American Journal of Biomedical Sciences*. 2012;**4**(1):50-59

[88] Katsuki H, Furuta S, Komarneni S. Microwave- versus conventional-hydrothermal synthesis of hydroxyapatite crystals from gypsum. *Journal of the American Ceramic Society*. 2004;**82**(8):2257-2259

[89] Wu Y-S, Chang W-K, Jou M. Hydroxyapatite synthesised from nanosized calcium carbonate via hydrothermal method. *Materials and Technologies*. 2012;**27**(1):119-123

[90] Macha I, Boonyang U, Cazalbou S, Ben-Nissan B, Charvillat C, Oktar F, et al. Comparative study of coral conversion, part 2: Microstructural evolution of calcium phosphate. *Journal of The Australian Ceramic Society*. 2015;**51**:149

[91] Felício-Fernandes G, Laranjeira MCM. Calcium phosphate biomaterials from marine algae. Hydrothermal synthesis and characterisation. *Química Nova*. 2000;**23**(4):441-446

[92] Macha IJ, Grossin D, Ben-Nissan B. Conversion of marine structures to calcium phosphate materials: Mechanisms of conversion using two

different phosphate solutions. Key Engineering Materials. 2016;**696**:36-39

[93] Xu Y, Wang D, Yang L, Tang H. Hydrothermal conversion of coral into hydroxyapatite. Materials Characterization. 2001;**47**(2):83-87

[94] Tampieri A, Sprio S, Ruffini A, Celotti G, Lesci IG, Roveri N. From wood to bone: Multi-step process to convert wood hierarchical structures into biomimetic hydroxyapatite scaffolds for bone tissue engineering. Journal of Materials Chemistry. 2009;**19**(28):4973

[95] Kuśnieruk S, Wojnarowicz J, Chodara A, Chudoba T, Gierlotka S, Lojkowski W. Influence of hydrothermal synthesis parameters on the properties of hydroxyapatite nanoparticles. Beilstein Journal of Nanotechnology. 2016;**7**:1586-1601

[96] Zhang H, Li S, Yan Y. Dissolution behavior of hydroxyapatite powder in hydrothermal solution. Ceramics International. 2001;**27**(4):451-454

[97] Du X, Chu Y, Xing S, Dong L. Hydrothermal synthesis of calcium hydroxyapatite nanorods in the presence of PVP. Journal of Materials Science. 2009;**44**(23):6273-6279

[98] Sadat-Shojai M, Atai M, Nodehi A, Khanlar LN. Hydroxyapatite nanorods as novel fillers for improving the properties of dental adhesives: Synthesis and application. Dental Materials. 2010;**26**(5):471-482

[99] Wang Y, Chen J, Wei K, Zhang S, Wang X. Surfactant-assisted synthesis of hydroxyapatite particles. Materials Letters. 2006;**60**(27):3227-3231